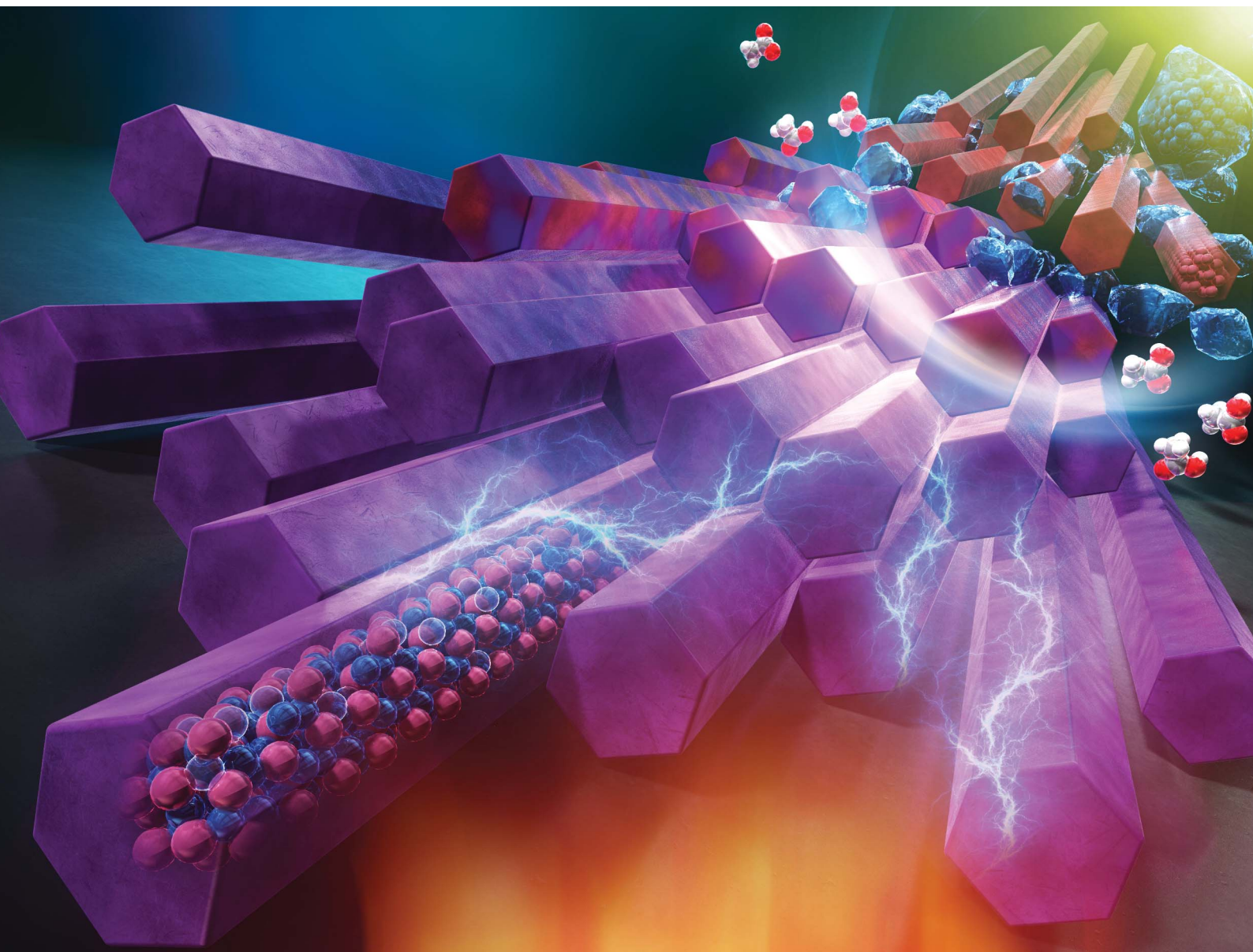


# Nanoscale Advances

Volume 6  
Number 13  
7 July 2024  
Pages 3243–3464

[rsc.li/nanoscale-advances](https://rsc.li/nanoscale-advances)



ISSN 2516-0230



## PAPER

Shunya Sakane, Hideki Tanaka *et al.*  
Precise synthesis of copper selenide nanowires with tailored Cu vacancies through photo-induced reduction for thermoelectric applications



Cite this: *Nanoscale Adv.*, 2024, 6, 3299

# Precise synthesis of copper selenide nanowires with tailored Cu vacancies through photo-induced reduction for thermoelectric applications†

Shunya Sakane,<sup>a</sup> Tatsuki Miura,<sup>b</sup> Kazuki Munakata,<sup>b</sup> Yusuke Morikawa,<sup>b</sup> Shunichiro Miwa,<sup>b</sup> Riku Yamanaka,<sup>c</sup> Toshiki Sugai,<sup>c</sup> Akito Ayukawa,<sup>a</sup> Haruhiko Udono<sup>a</sup> and Hideki Tanaka<sup>b</sup>

Nanostructuring in  $\alpha$ -Cu<sub>2</sub>Se while optimizing carrier concentration holds the promise of realizing further high thermoelectric performance at near room temperature. Nevertheless, controlling the amounts of Cu vacancies, which work as acceptors, in nanostructures is considerably more intricate than in bulk materials. Hence, controlling the amounts of Cu vacancies while maintaining the  $\alpha$ -phase and nanostructure shape poses a formidable challenge. In this study, we synthesized Cu<sub>2+x</sub>Se nanowires (NWs) with various amounts of Cu vacancies at room temperature by the photoreduction method and investigated their thermoelectric properties. Cu<sub>2+x</sub>Se NWs exhibited a comparable thermoelectric power factor to that of the polycrystalline films fabricated at higher temperature. The achievement of the high power factor despite low-temperature fabrication is attributed to the precise synthesis of Cu<sub>2+x</sub>Se NWs with various amounts of Cu vacancies. We also investigated the reaction process of Cu<sub>2.00</sub>Se NWs in detail by observing the reaction intermediates. It was found that photoreduction occurred with Cu<sup>2+</sup> ions adsorbed on Se NWs, leading to the reaction of Cu<sup>2+</sup> ions and Se NWs without Cu deficiency. Namely, this photoreduction under the adsorbed conditions realized the control of Cu vacancies in Cu<sub>2+x</sub>Se NWs.

Received 24th February 2024  
Accepted 24th April 2024

DOI: 10.1039/d4na00156g

rsc.li/nanoscale-advances

## Introduction

Thermoelectric conversion is one of the energy harvesting techniques. The efficiency monotonically increases with the thermoelectric figure of merit  $ZT (=S^2\sigma T/\kappa)$ , where  $S$  is the Seebeck coefficient,  $\sigma$  is the electrical conductivity,  $\kappa$  is the thermal conductivity, and  $T$  is the absolute temperature. To maximize thermoelectric performance of the material, it is effective to optimize carrier concentration and introduce nanostructures,<sup>1–21</sup> which can control phonon and carrier transport.

Cu<sub>2</sub>Se<sup>22–31</sup> is a promising thermoelectric material because it exhibits a high  $ZT$  of 0.68 at near room temperature (RT).<sup>22</sup> Therein, the carrier concentration is optimized to maximize the thermoelectric power factor ( $S^2\sigma$ ) by controlling the amounts of Cu vacancies, which work as acceptors. Nanostructuring while optimizing the carrier concentration holds the promise of realizing a higher thermoelectric performance. Nevertheless,

controlling the amounts of Cu vacancies in nanostructures is considerably more intricate than in bulk materials. When the amounts of Cu vacancies increase excessively in the nanostructures, they easily distort the structures of the  $\alpha$ -phase (semiconductor phase) until the rearrangement of the  $\beta$ -phase (metallic phase) is energetically favorable due to the larger contribution of the surface energy to the total energy of formation than that of bulk.<sup>32</sup> Hence, controlling the amounts of Cu vacancies while maintaining the  $\alpha$ -phase and nanostructure shape poses a formidable challenge. Furthermore, it is important to achieve high thermoelectric performance by controlling Cu vacancies with low-temperature synthesis to get practical advantages in applications such as flexible substrates with low heat resistance.

Recently, we developed the synthesis of single-phase  $\alpha$ -Cu<sub>2</sub>Se nanowires (NWs) through the photoreduction method. Our group synthesized size-controlled Cu nanoparticles by the photoreduction method,<sup>33–39</sup> where the slow reaction can control the morphology of copper nanoparticles.<sup>35</sup> We applied the above method to the synthesis of  $\alpha$ -Cu<sub>2</sub>Se NWs. Furthermore, we demonstrated  $S^2\sigma$  enhancement of poly(3,4-ethylenedioxythiophene): poly(styrene sulfonate) (PEDOT:PSS) by introduction of Cu<sub>2</sub>Se NWs.<sup>40</sup>

In this study, we synthesized Cu<sub>2+x</sub>Se NWs with various amounts of Cu vacancies by the photoreduction method at RT and systematically investigated their thermoelectric properties.

<sup>a</sup>Graduate School of Science and Engineering, Ibaraki University, 4-12-1, Nakanarusawa-cho, Hitachi, Ibaraki, 316-8511, Japan. E-mail: shunya.sakane.sz12@vc.ibaraki.ac.jp

<sup>b</sup>Faculty of Science and Engineering, Chuo University, 1-13-27, Kasuga, Bunkyo-ku, Tokyo, 112-8551, Japan. E-mail: htanaka@kc.chuo-u.ac.jp

<sup>c</sup>Faculty of Science, Toho University, 2-2-1, Miyama, Funabashi-shi, Chiba, 274-8510, Japan

† Electronic supplementary information (ESI) available. See DOI: <https://doi.org/10.1039/d4na00156g>



The thermoelectric properties were discussed in relation to Cu vacancies, which largely affect  $S^2\sigma$ . Furthermore, we elucidated the impact of the deliberately slow reduction process on achieving the precise synthesis of  $\text{Cu}_{2+x}\text{Se}$  NWs with various amounts of Cu vacancies by analyzing the reaction intermediates and providing a detailed discussion on the reaction kinetics.

## Experimental

### Synthesis of $\text{Cu}_{2+x}\text{Se}$ NWs

Se NWs were synthesized by the following method.<sup>41</sup>  $\text{SeO}_2$  (25 mg, FUJIFILM Wako Pure Chemical Corporation) and  $\beta$ -cyclodextrin (50 mg, FUJIFILM Wako Pure Chemical Corporation) were dissolved in 10 mL of Milli Q water and stirred under ultrasonication for 10 min. The solution was slowly added into L-ascorbic acid solution prepared with L-ascorbic acid (0.2000 g, Wako Pure Chemical Corporation) and Milli-Q water (10 mL) and was stirred for 4 hours. The mixed solution was centrifuged, and the resulting precipitates were washed with ethanol and Milli-Q water several times alternately. The precipitates were redispersed in ethanol without stirring for >4 hours, forming Se NWs as precipitates.

The synthesis method of  $\text{Cu}_2\text{Se}$  NWs is shown below. The Se NWs (10 mg) were dispersed in copper acetate solution prepared by dissolving 253  $\mu\text{mol}$  of copper acetate in aqueous solution containing 1 mL ethanol. The total volume of the dispersion thus obtained was adjusted to 10 mL by using Milli-Q water. The adjusted dispersion was irradiated using UV light (Hamamatsu Photonics: L9588-01A) with stirring for 12 hours, and  $\text{Cu}_2\text{Se}$  NWs were obtained as precipitates. The  $\text{Cu}_{2+x}\text{Se}$  NWs were also synthesized with some composition ratios ( $x = -0.05$ – $0.20$ ) by varying the amounts of copper acetate solution. To elucidate the reaction mechanism of  $\text{Cu}_2\text{Se}$  NWs through the photoreduction method,  $\text{Cu}_2\text{Se}$  NWs were also synthesized using UV light irradiation for 0–12 hours.

### Structural characterization of $\text{Cu}_{2+x}\text{Se}$ NWs

The crystal structures of the  $\text{Cu}_{2+x}\text{Se}$  NWs were characterized by powder X-ray diffraction (XRD) with an X-ray diffractometer (Rigaku, Smartlab), scanning electron microscopy (SEM)-energy dispersive X-ray spectroscopy (EDX) with a field-emission SEM (Hitachi High-Technologies, S-5500), and high-resolution transmission electron microscopy (HRTEM) with a TEM (Thermo Fisher Scientific, Tecnai G2 F20 S-TWIN, FEI). The composition ratios of  $\text{Cu}_{2+x}\text{Se}$  NWs were quantified by EDX, where the quantified excessive Cu amounts are defined to be  $x_q$  in this paper. The NW powders were also characterized by diffuse reflectance (DR) UV-vis spectrometry with a UV vis-NIR spectrometer (Shimadzu, UV-3600). The DR UV-vis-NIR spectra were obtained by using the Kubelka–Munk function  $F(R)$  to convert diffuse reflectance into an equivalent absorption coefficient, as follows:

$$F(R) = \frac{(1 - R)^2}{2R} \quad (1)$$

where  $R$  is the reflectance.

### Evaluation of thermoelectric properties of $\text{Cu}_{2+x}\text{NWs}$

The synthesized  $\text{Cu}_{2+x}\text{Se}$  NW powders were pressed at 160 MPa for 1 min to form  $\text{Cu}_{2+x}\text{Se}$  NW films at RT for the measurement of thermoelectric properties. The NW structures were maintained even after pressing (Fig. S1†).  $S$  was measured by using a ZEM-3 (ADVANCE RIKO) and  $\sigma$  was measured by the van der Pauw method at RT. Carrier concentration and carrier mobility were measured by Hall effect measurement (TOYO Corporation, M91-RTMG05).

## Results and discussion

Fig. 1a shows the SEM image for the obtained copper selenide NWs. The NW structures were observed and the diameter and length of the NWs were  $300 \pm 100$  nm and  $10 \pm 5$   $\mu\text{m}$ , respectively (Fig. S2†). Since these values were almost the same as those of the Se NWs,<sup>40</sup> it is considered that copper selenide was formed directly on the Se NWs by photoreduction. Fig. 1b shows the HRTEM image of the NWs. The lattice spacings of monoclinic  $\alpha$ - $\text{Cu}_2\text{Se}$  (400) and (090) were observed, which correspond to the circles in the fast Fourier transformation (FFT) image (Fig. 1c). Analysis results of various regions of NWs indicate that the obtained NWs were composed of polycrystalline  $\alpha$ - $\text{Cu}_2\text{Se}$ .

Fig. 1d–f show the SEM-EDX mapping images. A bundle of multiple NWs was used for the EDX analysis to obtain a strong signal, as shown in Fig. 1d. From the mapping images, Cu and Se species were observed on NWs. To clarify the uniformity of constituent elements on NWs, line profiles in Fig. 1g were obtained for a line segment A and B in Fig. 1e and f. The intensity of Cu and Se species rose and dropped at the same position indicated by arrows. This indicates that Cu species were uniformly distributed along Se species on NWs.

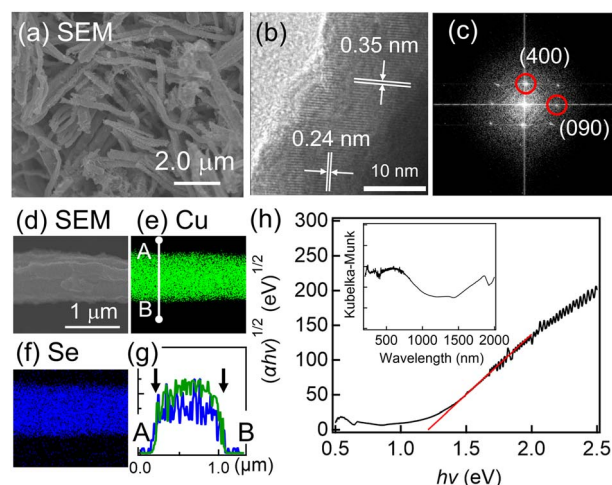


Fig. 1 Characterization of copper selenide NWs synthesized using UV light irradiation for 12 hours. (a) A SEM image, (b) a HRTEM image, and (c) a FFT pattern. The arrows in (b) indicate lattice spacings of  $\alpha$ - $\text{Cu}_2\text{Se}$ , corresponding to the  $\alpha$ - $\text{Cu}_2\text{Se}$  (400) and (090) spots in (c). (d) SEM image and EDX mappings of (e) Cu and (f) Se. (g) Line profiles for a line segment A and B in (e). The green and blue profiles represent Cu and Se, respectively. (h) A plot of  $(\alpha h\nu)^{1/2}$  versus  $h\nu$  calculated from the DR UV-vis spectrum in the inset graph.



The DR UV-vis-NIR spectrum of the  $\alpha$ -Cu<sub>2</sub>Se NWs is shown in the inset of Fig. 1h, which indicates that the  $\alpha$ -Cu<sub>2</sub>Se NWs exhibited optical absorption at a wavelength of <1000 nm. The optical absorption near the band edge follows the equation:<sup>42</sup>

$$\alpha h\nu = A(h\nu - E_g)^{n/2} \quad (2)$$

where  $\alpha$ ,  $h$ ,  $\nu$ ,  $E_g$  and  $A$  are the absorption coefficient, Planck's constant, light frequency, band gap energy, and a constant, respectively. Among them,  $\nu$  depends on the transition process in a semiconductor, such as  $n = 1$  or  $n = 4$  for direct transition or indirect transition, respectively. For  $\alpha$ -Cu<sub>2</sub>Se, the value of  $n$  is 4 for indirect transition. The  $E_g$  value of  $\alpha$ -Cu<sub>2</sub>Se NWs was estimated to be 1.20 eV from a plot of  $(\alpha h\nu)^{1/2}$  versus photon energy ( $h\nu$ ) in Fig. 1h. This value is in good agreement with that of bulk  $\alpha$ -Cu<sub>2</sub>Se ( $\sim 1.2$  eV<sup>30,43</sup>). Considering that even a small amount of impurity changes the band gap of Cu<sub>2</sub>Se,<sup>44</sup> this result indicates that the pure  $\alpha$ -Cu<sub>2</sub>Se NWs were precisely formed by the photoreduction method.

Cu<sub>2+x</sub>Se NWs were also synthesized with various composition ratios. As shown in Fig. 2a, the composition ratio quantified by EDX ( $x_q$ ) exhibits a monotonically increasing trend in relation to  $x$ . This trend suggests the formation of Cu<sub>2+x</sub>Se NWs with various composition ratios. However, in the range of  $x > 0.0$ , the  $x_q$  values were saturated and were consistently smaller than the corresponding  $x$  values. The missing Cu remained unreacted in solution, namely only Cu that can be soluble in Cu<sub>2</sub>Se reacted. Here, to investigate the presence and amounts of Cu vacancies in Cu<sub>2+x</sub>Se NWs, we obtained DR UV-vis-NIR spectra of these NWs. Fig. 2b shows the DR UV-vis-NIR spectra normalized by using the Kubelka–Munk values at around a 500 nm wavelength corresponding to band-edge or interband absorption.<sup>45</sup> For  $x \leq 0.0$ , additional broad peaks were observed at a longer wavelength than 800 nm, corresponding to intraband absorption.<sup>45</sup> Intraband absorption is caused by electron excitation from a lower energy filled state to a higher energy empty state within the valence band, which is formed by the introduction of Cu vacancies.<sup>45</sup> The intraband absorption peak (Cu vacancies) decreased on increasing  $x$  in Cu<sub>2+x</sub>Se NWs, as shown in Fig. 2b. Although there are small amounts of Cu vacancies for Cu<sub>2.00</sub>Se, the Cu vacancies almost

disappeared for Cu<sub>2.10</sub>Se by adding a slight excess of Cu. The saturation of  $x_q$  (Fig. 2a) was found to be due to the reduction of Cu vacancies brought about by the incorporation of excess Cu. The Cu vacancies affect the carrier concentrations ( $p$ ) in Cu<sub>2+x</sub>Se NWs because Cu vacancies work as acceptors in Cu<sub>2</sub>Se. In fact, the  $p$  value of Cu<sub>1.95</sub>Se NWs ( $6.1 \times 10^{21}$  cm<sup>-3</sup>) measured by Hall effect measurement was higher than that of Cu<sub>2.00</sub>Se NWs ( $1.8 \times 10^{21}$  cm<sup>-3</sup>). This result also supports the decrease in the amounts of Cu vacancies in Cu<sub>2+x</sub>Se NWs on increasing  $x$ . From these results, Cu<sub>2+x</sub>Se NWs were precisely synthesized with various composition ratios by the photoreduction method.

Fig. 3a–c show the composition ratio ( $x$ ) dependencies of  $\sigma$ ,  $S$  and  $S^2\sigma$  of Cu<sub>2+x</sub>Se NWs measured at RT, respectively.  $\sigma$  and  $S$  of Cu<sub>2+x</sub>Se NWs monotonically decreased and increased as  $x$  increased, respectively. As a result,  $S^2\sigma$  was maximized for Cu<sub>2.00</sub>Se NWs. The dependencies can be explained by the change in  $p$  in Cu<sub>2+x</sub>Se NWs. In general, there is a trade-off relationship between  $\sigma$  and  $S$ :  $\sigma$  increases and  $S$  decreases with the increase in  $p$ , and  $S^2\sigma$  is maximized on optimizing  $p$ . In the case of Cu<sub>2+x</sub>Se NWs,  $S^2\sigma$  was maximized by precisely synthesizing Cu<sub>2+x</sub>Se NWs with various composition ratios because  $p$  depends on the amounts of Cu vacancies. We abandoned the measurement of  $\kappa$  due to the subtle thickness and surface roughness of the Cu<sub>2+x</sub>Se NW films. However,  $\kappa$  of our Cu<sub>2+x</sub>Se NW films might be lower than that of Cu<sub>2</sub>Se bulks with uniform nanostructures because phonons with various mean free paths can be scattered at two types of interfaces: (1) polycrystalline interfaces and (2) NW/NW interfaces. The actual  $\kappa$  will be evaluated in future study.

Comparing the thermoelectric properties of Cu<sub>2+x</sub>Se NWs with those of previously reported bulk samples,  $S$  was comparable to that of the bulk samples while carrier mobility  $\mu$  was

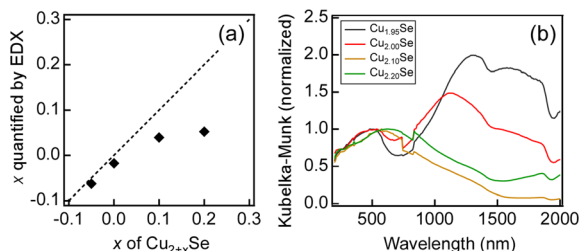


Fig. 2 (a) The composition ratio quantified by EDX ( $x_q$ ) as a function of composition ratio ( $x$ ). The dashed line in (a) indicates the theoretical one when  $x_q$  is the same as  $x$ . (b) DR UV-vis-NIR spectra of Cu<sub>2+x</sub>Se NWs normalized by using the Kubelka–Munk values at around a 500 nm wavelength corresponding to band-edge or interband absorption.

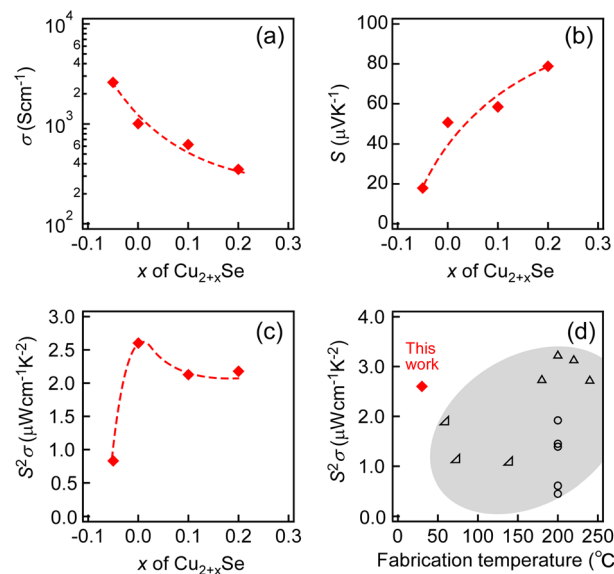


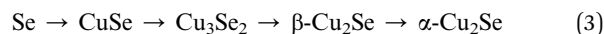
Fig. 3 The composition ratio ( $x$ ) dependencies of (a)  $\sigma$ , (b)  $S$  and (c)  $S^2\sigma$  of Cu<sub>2+x</sub>Se NWs measured at RT. The dashed lines in a–c indicate eye-guides. (d)  $S^2\sigma$  of Cu<sub>2.00</sub>Se NWs (solid symbol) as a function of the fabrication temperature. In (d), the data of polycrystalline films (open symbol)<sup>48–50</sup> were plotted.



lower than that of the bulk samples at the same carrier concentration<sup>22,46</sup> (Fig. S3†). In general, the bulk samples synthesized at high temperature by the sintering or melting method exhibit higher carrier mobility due to low concentration of point defects and polycrystalline interfaces.<sup>47</sup> In fact, bulk Cu<sub>2</sub>Se samples exhibit a high  $S^2\sigma$  of  $\sim 8 \mu\text{W cm}^{-1} \text{K}^{-2}$  at RT.<sup>22</sup> To compare our Cu<sub>2+x</sub>Se NW samples synthesized at near RT with previously reported samples, we plotted  $S^2\sigma$  data with thin films fabricated at relatively low temperature as a function of fabrication temperature as shown in Fig. 3d. Cu<sub>2+x</sub>Se NW samples exhibited comparable  $S^2\sigma$  to that of the polycrystalline films fabricated at higher temperature.<sup>48–50</sup> The achievement of the high  $S^2\sigma$  despite low-temperature fabrication is attributed to the precise synthesis of Cu<sub>2+x</sub>Se NWs with various amounts of Cu vacancies. The  $S^2\sigma$  values also followed the temperature trend of epitaxial films (Fig. S4†).<sup>51</sup> Here, we suggest that the reason why Cu<sub>2+x</sub>Se NWs could be synthesized with various Cu vacancies is due to the precise reaction of Cu<sup>2+</sup> and Se nanowires without additional Cu-related precipitates coming from the slow reaction of photoreduction. In the following section, we investigated the reaction process of Cu<sub>2.00</sub>Se NWs in detail by observing the reaction intermediates.

Reaction time dependences of  $2\theta$ - $\omega$  scans of XRD for Cu<sub>2.00</sub>Se NWs were observed as shown in Fig. S5.† To see the reaction time dependence simply, the enlarged graph of 20–35° was used for the analysis, as shown in Fig. 4a. The peaks indicated by star marks (★) for 12 h were found to be assigned to monoclinic  $\alpha$ -Cu<sub>2</sub>Se. Since the observed pattern was entirely different from that for 0 h (as-prepared Se NWs) assigned to hexagonal Se, Se NWs completely reacted with Cu<sup>2+</sup> ions for 12 h. No peaks originating from metallic Cu at 43.3°, Cu<sub>2</sub>O at 36.4° or CuO at 35.5° were observed (JCPDS file no. 5-0667 and 48-1548)

(Fig. S5†). Looking at the XRD patterns for 0.5–6 h, various phases (hexagonal Se (●), hexagonal CuSe (▼), tetragonal Cu<sub>3</sub>Se<sub>2</sub> (■), cubic  $\beta$ -Cu<sub>2</sub>Se (▲), and monoclinic  $\alpha$ -Cu<sub>2</sub>Se (★)) were observed. From these XRD patterns, typical peaks originating from CuSe + Se, Cu<sub>3</sub>Se<sub>2</sub> + CuSe +  $\beta$ -Cu<sub>2</sub>Se,  $\beta$ -Cu<sub>2</sub>Se + Cu<sub>3</sub>Se<sub>2</sub>,  $\alpha$ -Cu<sub>2</sub>Se, and  $\alpha$ -Cu<sub>2</sub>Se were observed for 0.5, 2, 4, 6, and 12 h, respectively (Fig. 4b). Considering that the main peaks for 0.5, 2, 4, and 6 h were assigned to CuSe, Cu<sub>3</sub>Se<sub>2</sub>,  $\beta$ -Cu<sub>2</sub>Se, and  $\alpha$ -Cu<sub>2</sub>Se, respectively, Se NWs were sequentially reacted with Cu<sup>2+</sup> ions as follows:



As these results show,  $\alpha$ -Cu<sub>2</sub>Se NWs were formed through crystal structure changes by a sequential reaction as indicated by eqn (3). This sequential reaction of copper and selenium was also reported for the synthesis of copper selenides by the electrochemical method.<sup>52,53</sup> It was found that similar reaction processes occurred for the synthesis of  $\alpha$ -Cu<sub>2</sub>Se NWs through the photoreduction method. This result indicates that Cu<sup>2+</sup> and Se NWs were precisely reacted without additional Cu-related precipitates, leading to the control of the amounts of Cu vacancies. Since the Cu<sub>2+x</sub>Se NWs used for the evaluations of thermoelectric properties and UV-vis-NIR were synthesized at 12 h, they were probably completely alloyed.

We also synthesized single phase  $\beta$ -Cu<sub>2</sub>Se or CuSe NWs with the Cu/Se atomic ratios of 1.8 or 1.0 by the photoreduction method, respectively.  $2\theta$ - $\omega$  XRD scans of these NWs are shown in Fig. S6.† The XRD peaks observed from NWs with a Cu/Se ratio of 1.8 and 1.0 were assigned to only cubic  $\beta$ -Cu<sub>2</sub>Se and hexagonal CuSe, respectively. This result indicates that targeted phases of copper selenide can be synthesized by adjusting Cu/Se ratios. We also found that  $S^2\sigma$  of  $\beta$ -Cu<sub>2</sub>Se NWs and CuSe NWs was much lower than that of  $\alpha$ -Cu<sub>2</sub>Se NWs (Fig. S7†). Namely, the control of the crystalline phase through the photoreduction method is one of the reasons why  $\alpha$ -Cu<sub>2</sub>Se NWs exhibited a high  $S^2\sigma$  in this study.

To elucidate the process of the reaction of Cu<sup>2+</sup> ions and Se NWs, the reaction kinetics are discussed below. Cu/Se atomic ratios obtained by quantitative EDX analysis were plotted as a function of reaction time (Fig. 4c). The ratio was almost saturated to be  $\sim 2$  at 6 h. This result is consistent with XRD results, where single-phase  $\alpha$ -Cu<sub>2</sub>Se was formed at 6 h. It is obvious that the Cu/Se data can be fitted using the following equation:

$$\text{Cu/Se} = 2(1 - \exp(-kt)) \quad (4)$$

where  $t$  is the reaction time and  $k$  is the reaction rate. The fitting parameter,  $k$  was found to be 0.46 (h<sup>-1</sup>), where the initial value of Cu/Se was set to 0 ( $t = 0$ ). The dependence in eqn (4) seems to be explained by the following two-step reaction: the rate-determining step (5) and the subsequent fast step (6)

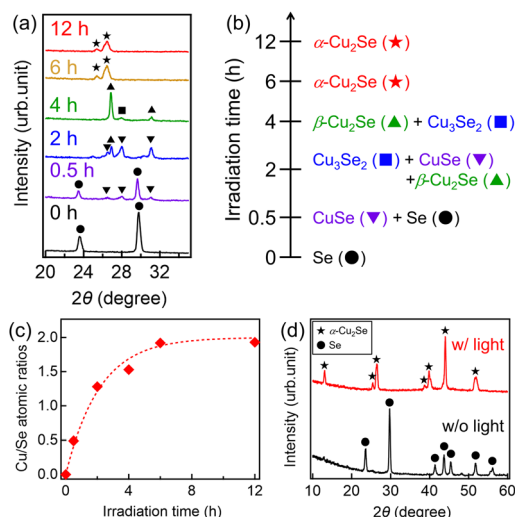


Fig. 4 (a)  $2\theta$ - $\omega$  XRD scans for copper selenide NWs synthesized using UV light irradiation for 0–12 hours. (b) Crystal phases of copper selenide NWs as a function of light irradiation time. (c) Cu/Se atomic ratios obtained by quantitative EDX analysis as a function of light irradiation time. In (c), the dashed curve represents the fitted one to the experimental data with eqn (6). (d)  $2\theta$ - $\omega$  XRD scans for the samples with and without light irradiation for 12 hours.



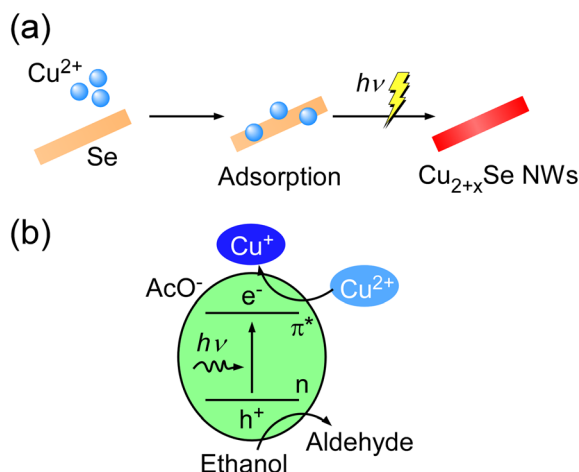
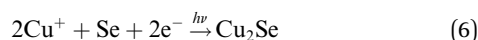


Fig. 5 Schematic illustration of (a) the precise synthesis of  $\text{Cu}_{2+x}\text{Se}$  NWs through photoreduction with  $\text{Cu}^{2+}$  ions adsorbed on Se NWs and (b) the photoreduction mechanism of  $\text{Cu}^{2+}$  ions.



To investigate the effect of light irradiation, the same synthesis processes without light irradiation for 12 hours were also conducted. Fig. 4d shows  $2\theta$ - $\omega$  XRD scans for samples with and without light irradiation for 12 hours. In the sample without light irradiation, XRD patterns of only hexagonal Se were observed while those of other copper selenides such as monoclinic  $\alpha$ - $\text{Cu}_2\text{Se}$  were not observed. Thus,  $\text{Cu}^{2+}$  ions and Se NWs could not be reacted without light irradiation. Therefore, these results support that photoreduction occurred with  $\text{Cu}^+$  ions adsorbed on Se NWs, as shown in Fig. 5a. Therefore,  $\text{Cu}^{2+}$  ions were sequentially reacted with Se NWs without deficiency. Namely, this photoreduction under the adsorbed conditions realized the control of Cu vacancies in  $\text{Cu}_{2+x}\text{Se}$  NWs (Fig. 5a).

Finally, we show the mechanism of the photoreduction process. In our previous studies, Cu nanoparticles were synthesized by reducing copper ions through the photoreduction method.<sup>33</sup> Therein, we consider that photoinduced electrons in acetic acid ions ( $\text{AcO}^-$ ) were transferred to copper ions according to the previous studies on the photoredox properties of copper(II)-carboxylate complexes.<sup>54–57</sup> Given the consistent use of the same solvent (water and ethanol) and cuprous salt (copper acetate) in this study, the reduction of copper ions comes from the same mechanism observed in Cu nanoparticle formation, as illustrated in Fig. 5b. Notably, considering that the selenium valence in  $\alpha$ - $\text{Cu}_2\text{Se}$  is  $-2$ ,<sup>50,58</sup> it is obvious that Se was also reduced by light irradiation.

## Conclusions

We synthesized  $\text{Cu}_{2+x}\text{Se}$  NWs with various amounts of Cu vacancies at RT by the photoreduction method and investigated their thermoelectric properties.  $\text{Cu}_{2+x}\text{Se}$  NWs exhibited comparable  $S^2\sigma$  to that of the polycrystalline films fabricated at higher temperature. The achievement of the high  $S^2\sigma$  despite

low-temperature fabrication is attributed to the precise synthesis of  $\text{Cu}_{2+x}\text{Se}$  NWs with various amounts of Cu vacancies. From XRD analysis of the intermediate condition before complete reaction, it was found that Se NWs were consequently reacted with  $\text{Cu}^{2+}$  ions, accompanying changes in crystal structures, resulting in the formation of single-phase  $\alpha$ - $\text{Cu}_2\text{Se}$  NWs. Furthermore, the discussion of reaction kinetics revealed that photoreduction occurred with  $\text{Cu}^{2+}$  ions adsorbed on Se NWs. Therefore,  $\text{Cu}^{2+}$  ions were sequentially reacted with Se NWs without deficiency. Namely, this photoreduction under the adsorbed conditions realized the control of Cu vacancies in  $\text{Cu}_{2+x}\text{Se}$  NWs.

## Author contributions

S. S. conceptualization, methodology, formal analysis, funding acquisition, visualization, writing – original draft, writing – review & editing, T. M. data curation, investigation, K. M. data curation, investigation, Y. M. data curation, investigation, S. M. data curation, investigation, R. Y. data curation, T. S. data curation, A. A. data curation, H. U. writing – review & editing, and H. T. funding acquisition, supervision, writing – review & editing.

## Conflicts of interest

There are no conflicts to declare.

## Acknowledgements

This work was supported by Grant-in-Aid for Early-Career Scientists Grant Number 21K14479 and Grant-in-Aid for Scientific Research (C) Grant Number 19K05187 from JSPS KAKENHI, Japan. We are thankful for the assistance of Prof. K. Ohishi and Prof. H. Chang at Chuo University for cold pressing and XRD measurement, respectively.

## References

- W. Liu, X. Yan, G. Chen and Z. Ren, Recent Advances in Thermoelectric Nanocomposites, *Nano Energy*, 2012, **1**, 42–56.
- S. K. Bux, R. G. Blair, P. K. Gogna, H. Lee, G. Chen, M. S. Dresselhaus, R. B. Kaner and J. P. Fleurial, Nanostructured Bulk Silicon as an Effective Thermoelectric Material, *Adv. Funct. Mater.*, 2009, **19**, 2445–2452.
- A. I. Hochbaum, R. Chen, R. D. Delgado, W. Liang, E. C. Garnett, M. Najarian, A. Majumdar and P. Yang, Enhanced Thermoelectric Performance of Rough Silicon Nanowires, *Nature*, 2008, **451**, 163–167.
- A. I. Boukai, Y. Bunimovich, J. T. Kheli, J. K. Yu, W. A. Goddard and J. R. Heath, Silicon Nanowires as Efficient Thermoelectric Materials, *Nature*, 2008, **451**, 168–171.
- G. Joshi, H. Lee, Y. Lan, X. Wang, G. Zhu, D. Wang, R. W. Gould, D. C. Cuff, M. Y. Tang, M. S. Dresselhaus, G. Chen and Z. Ren, Enhanced Thermoelectric Figure-of-



- Merit in Nanostructured p-type Silicon Germanium Bulk Alloys, *Nano Lett.*, 2008, **8**, 4670–4674.
- 6 X. W. Wang, H. Lee, Y. C. Lan, G. H. Zhu, G. Joshi, D. Z. Wang, J. Yang, A. J. Muto, M. Y. Tang, J. Klatsky, S. Song, M. S. Dresselhaus, G. Chen and Z. F. Ren, Enhanced Thermoelectric Figure of Merit in Nanostructured n-type Silicon Germanium Bulk Alloy, *Appl. Phys. Lett.*, 2008, **93**, 193121.
- 7 K. Biswas, J. He, I. D. Blum, C. I. Wu, T. P. Hogan, D. N. Seidman, V. P. Dravid and M. G. Kanatzidis, High-performance Bulk Thermoelectrics with All-scale Hierarchical Architectures, *Nature*, 2012, **489**, 414–418.
- 8 Y. Nakamura, M. Isogawa, T. Ueda, S. Yamasaka, H. Matsui, J. Kikkawa, S. Ikeuchi, T. Oyake, T. Hori, J. Shiomi and A. Sakai, Anomalous Reduction of Thermal Conductivity in Coherent Nanocrystal Architecture for Silicon Thermoelectric Material, *Nano Energy*, 2015, **12**, 845–851.
- 9 Y. Nakamura, Nanostructure Design for Drastic Reduction of Thermal Conductivity While Preserving High Electrical Conductivity, *Sci. Technol. Adv. Mater.*, 2018, **19**, 31–43.
- 10 X. Zianni and D. Narducci, Synergy between Defects, Charge Neutrality and Energy Filtering in Hyper-doped Nanocrystalline Materials for High Thermoelectric Efficiency, *Nanoscale*, 2019, **11**, 7667.
- 11 K. Biswas, J. He, Q. Zhang, G. Wang, C. Uher, V. P. Dravid and M. G. Kanatzidis, Strained Endotaxial Nanostructures with High Thermoelectric Figure of Merit, *Nat. Chem.*, 2011, **3**, 160–166.
- 12 D. Souda, K. Shimizu, Y. Ohishi, H. Muta, T. Yagi and K. Kurosaki, High Thermoelectric Power Factor of Si-Mg<sub>2</sub>Si Nanocomposite Ribbons Synthesized by Melt Spinning, *ACS Appl. Energy Mater.*, 2020, **3**, 1962–1968.
- 13 M. Nomura, R. Anufriev, Z. Zhang, J. Maire, Y. Guo, R. Yanagisawa and S. Volz, Review of Thermal Transport in Phononic Crystals, *Mater. Today Phys.*, 2022, **22**, 100613.
- 14 S. Yamasaka, Y. Nakamura, T. Ueda, S. Takeuchi and A. Sakai, Phonon Transport Control by Nanoarchitecture Including Epitaxial Ge Nanodots for Si-based Thermoelectric Materials, *Sci. Rep.*, 2015, **5**, 14490.
- 15 R. Anufriev, A. Ramiere, J. Maire and M. Nomura, Heat Guiding and Focusing Using Ballistic Phonon Transport in Phononic Nanostructures, *Nat. Commun.*, 2017, **8**, 15505.
- 16 S. Sakane, T. Ishibe, K. Mizuta, M. Kashino, K. Watanabe, T. Fujita, Y. Kamakura, N. Mori and Y. Nakamura, Methodology of Thermoelectric Power Factor Enhancement by Nanoscale Thermal Management in Bulk SiGe Composites, *ACS Appl. Energy Mater.*, 2020, **3**, 1235–1241.
- 17 S. Sakane, T. Ishibe, K. Mizuta, T. Fujita, Y. Kiyofuji, J. Ohe, E. Kobayashi and Y. Nakamura, Anomalous Enhancement of Thermoelectric Power Factor by Thermal Management with Resonant Level Effect, *J. Mater. Chem. A*, 2021, **9**, 4851–4857.
- 18 D. Vashaee and A. Shakouri, Improved Thermoelectric Power Factor in Metal-Based Superlattices, *Phys. Rev. Lett.*, 2004, **92**, 106103.
- 19 T. Ishibe, A. Tomeda, K. Watanabe, Y. Kamakura, N. Mori, N. Naruse, Y. Mera, Y. Yamashita and Y. Nakamura, Methodology of Thermoelectric Power Factor Enhancement by Controlling Nanowire Interface, *ACS Appl. Mater. Interfaces*, 2018, **10**, 37709–37716.
- 20 S. Sakane, T. Ishibe, T. Taniguchi, N. Naruse, Y. Mera, T. Fujita, M. M. Alam, K. Sawano, N. Mori and Y. Nakamura, Thermoelectric Power Factor Enhancement Based on Carrier Transport Physics in Ultimately Phonon-Controlled Si Nanostructures, *Mater. Today Energy*, 2019, **13**, 56–63.
- 21 S. Sakane, T. Ishibe, Y. Yukawa and Y. Nakamura, Thermoelectric Properties of B-doped Nanostructured Bulk Diamond with Lowered Thermal Conductivity, *Diam. Relat. Mater.*, 2023, **140**, 110410.
- 22 J. Y. Tak, W. H. Nam, C. Lee, S. Kim, Y. S. Lim, K. Ko, S. Lee, W. S. Seo, H. K. Cho, J. H. Shim and C. H. Park, Ultralow Lattice Thermal Conductivity and Significantly Enhanced Near-Room-Temperature Thermoelectric Figure of Merit in  $\alpha$ -Cu<sub>2</sub>Se through Suppressed Cu Vacancy Formation by Overstoichiometric Cu Addition, *Chem. Mater.*, 2018, **30**, 3276–3284.
- 23 S. D. Kang, S. A. Danilkin, U. Aydemir, M. Avdeev, A. Studer and G. J. Snyder, Apparent Critical Phenomena in the Superionic Phase Transition of Cu<sub>2-x</sub>Se, *New J. Phys.*, 2016, **18**, 013024.
- 24 W. D. Liu, L. Yang, Z. G. Chen and J. Zou, Promising and Eco-Friendly Cu<sub>2</sub>X-Based Thermoelectric Materials: Progress and Applications, *Adv. Mater.*, 2020, **32**, 1905703.
- 25 Z. Zhang, K. Zhao, T. R. Wei, P. Qiu, L. Chen and X. Shi, Cu<sub>2</sub>Se-Based Liquid-like Thermoelectric Materials: Looking Back and Stepping Forward, *Energy Environ. Sci.*, 2020, **13**, 3307–3329.
- 26 Y. Qin, L. Yang, J. Wei, S. Yang, M. Zhang, X. Wang and F. Yang, Doping Effect on Cu<sub>2</sub>Se Thermoelectric Performance: A Review, *Materials*, 2020, **13**, 5704.
- 27 S. M. K. N. Islam, M. B. Cortie and X. Wang, Grape Juice: an Effective Liquid Additive for Significant Enhancement of Thermoelectric Performance of Cu<sub>2</sub>Se, *J. Mater. Chem. A*, 2020, **8**, 16913.
- 28 N. Chen, M. R. Scimeca, S. J. Paul, S. B. Hafiz, Z. Yang, X. Liu, F. Yang, D. K. Ko and A. Sahu, High-performance Thermoelectric Silver Selenide Thin Films Cation Exchanged From a Copper Selenide Template, *Nanoscale Adv.*, 2020, **2**, 368.
- 29 L. Yang, Z. G. Chen, G. Han, M. Hong, Y. Zou and J. Zou, High-Performance Thermoelectric Cu<sub>2</sub>Se Nanoplates Through Nanostructure Engineering, *Nano Energy*, 2015, **16**, 367–374.
- 30 H. Liu, X. Shi, F. Xu, L. Zhang, W. Zhang, L. Chen, Q. Li, C. Uher, T. Day and G. J. Snyder, Copper Ion Liquid-Like Thermoelectrics, *Nat. Mater.*, 2012, **11**, 422–425.
- 31 B. Yu, W. Liu, S. Chen, H. Wang, H. Wang, G. Chen and Z. Ren, Thermoelectric Properties of Copper Selenide with Ordered Selenium Layer and Disordered Copper Layer, *Nano Energy*, 2012, **1**, 472–478.
- 32 S. Deka, A. Genovese, Y. Zhang, K. Miszta, G. Bertoni, R. Krahne, C. Giannini and L. Manna, Phosphine-Free Synthesis of p-Type Copper(I) Selenide Nanocrystals in Hot Coordinating Solvents, *J. Am. Chem. Soc.*, 2010, **132**, 8913.



- 33 M. Miyagawa, T. Maeda, R. Tokuda, A. Shibusawa, T. Aoki, K. Okumura and H. Tanaka, Precious Metal-like Oxide-Free Copper Nanoparticles: High Oxidation Resistance and Geometric Structure, *RSC Adv.*, 2016, **6**, 104560–104565.
- 34 M. Miyagawa, A. Shibusawa, K. Maeda, A. Tashiro, T. Sugai and H. Tanaka, Diameter-Controlled Cu Nanoparticles on Saponite and Preparation of Film by Using Spontaneous Phase Separation, *RSC Adv.*, 2017, **7**, 41896.
- 35 M. Miyagawa, M. Usui, Y. Imura, S. Kuwahara, T. Sugai and H. Tanaka, Aqueous Synthesis of Protectant-Free Copper Nanocubes by a Disproportionation Reaction of Cu<sub>2</sub>O on Synthetic Saponite, *Chem. Commun.*, 2018, **54**, 8454.
- 36 M. Miyagawa, Y. Ikeyama, H. Kotake, T. Maeda and H. Tanaka, Environmental-Friendly Degradation of Clay-Hybridized Cu Nanoparticles by Carboxylic Acids, *Chem. Phys. Lett.*, 2020, **753**, 137615.
- 37 M. Miyagawa, K. Nishino, A. Shibusawa, H. Kotake and H. Tanaka, Plasmonic Photoluminescence of Cu Nanoparticle Realized by Molecular Optical Antenna Designed on Nanosheets, *Chem. Lett.*, 2022, **51**, 500–503.
- 38 S. Sakane, T. Anji, I. Yamagishi, I. Kohara and H. Tanaka, Plasmonic Heating of Copper Nanoparticles with Thermoresponsive Polymers, *Chem. Lett.*, 2023, **52**, 582–585.
- 39 S. Sakane, K. Akimoto, K. Konishi, K. Takaoka, H. Iwatsuki, M. Akutsu, T. Sugai and H. Tanaka, Catalytic Activity of Non-aggregating Cu Nanoparticles Supported in Pores of Zeolite for Aerobic Oxidation of Benzyl Alcohol, *ACS Omega*, 2024, **9**, 970–976.
- 40 S. Sakane, S. Miwa, T. Miura, K. Munakata, T. Ishide, Y. Nakamura and H. Tanaka, Thermoelectric Properties of PEDOT:PSS Containing Connected Copper Selenide Nanowires Synthesized by the Photoreduction Method, *ACS Omega*, 2022, **7**, 32101–32107.
- 41 Q. Li and V. W. W. Yam, High-yield Synthesis of Selenium Nanowires in Water at Room Temperature, *Chem. Commun.*, 2006, 1006–1008.
- 42 B. Liu, L. Ning, H. Zhao, C. Zhang, H. Yang and S. Liu, Visible-light Photocatalysis in Cu<sub>2</sub>Se Nanowires with Exposed {111} Facets and Charge Separation Between (111) and ( $\bar{1}\bar{1}\bar{1}$ ) Polar Surfaces, *Phys. Chem. Chem. Phys.*, 2015, **17**, 13280–13289.
- 43 Y. You, H. Hu and J. H. Choi, Atomic Adsorption on Monolayer Cu<sub>2</sub>Se: A First-Principles Study, *Phys. Chem. Chem. Phys.*, 2021, **23**, 9814–9821.
- 44 A. P. Sudha, P. Prema, J. Henry, K. Mohanraj and G. Sivakumar, Influence of Trivalent (Bi, Sb) Metal Ions on the Photosensitivity of Doped Cu<sub>2</sub>Se Thin Films, *J. Mater. Sci. Mater. Electron.*, 2017, **28**, 6379–6387.
- 45 M. R. Scimeca, F. Yang, E. Zaia, N. Chen, P. Zhao, M. P. Gordon, J. D. Forster, Y. S. Liu, J. Guo, J. J. Urban and A. Sahu, Rapid Stoichiometry Control in Cu<sub>2</sub>Se Thin Films for Room-Temperature Power Factor Improvement, *ACS Appl. Energy Mater.*, 2019, **2**, 1517–1525.
- 46 J. Yu, K. Zhao, P. Qiu, X. Shi and L. Chen, Thermoelectric Properties of Copper-Deficient Cu<sub>2-x</sub>Se (0.05 ≤ x ≤ 0.25) Binary Compounds, *Ceram. Int.*, 2017, **43**, 11142–11148.
- 47 S. Sakane, T. Ishibe, T. Hinakawa, N. Naruse, Y. Mera, M. M. Alam, K. Sawano and Y. Nakamura, High Thermoelectric Performance in High Crystallinity Epitaxial Si Films Containing Silicide Nanodots with Low Thermal Conductivity, *Appl. Phys. Lett.*, 2019, **115**, 182104.
- 48 Y. Li, Y. Zhong, D. Zhang, J. Niu, M. Nisar, M. Wei, G. Liang, P. Fan and Z. Zheng, Enhanced Thermoelectric Properties of Cu<sub>2</sub>Se Flexible Thin Films by Optimizing Growth Temperature and Elemental Composition, *ACS Appl. Energy Mater.*, 2022, **5**, 13964–13970.
- 49 P. Fan, X. Huang, T. Chen, F. Li, Y. Chen, B. Jabar, S. Chen, H. Ma, G. Liang, J. Luo, X. Zhang and Z. Zheng,  $\alpha$ -Cu<sub>2</sub>Se Thermoelectric Thin Films Prepared by Copper Sputtering into Selenium Precursor Layers, *Chem. Eng. J.*, 2021, **410**, 128444.
- 50 L. Yang, J. Wei, Y. Qin, L. Wei, P. Song, M. Zhang, F. Yang and X. Wang, Thermoelectric Properties of Cu<sub>2</sub>Se Nano-Thin Film by Magnetron Sputtering, *Materials*, 2021, **14**, 2075.
- 51 A. Wang, Y. Xue, J. Wang, X. Yang, J. Wang, Z. Li and S. Wang, High Thermoelectric Performance of Cu<sub>2</sub>Se-Based Thin Films with Adjustable Element Ratios by Pulsed Laser Deposition, *Mater. Today Energy*, 2022, **24**, 100929.
- 52 C. Dai, L. Hu, H. Chen, X. Jin, Y. Han, Y. Wang, X. Li, X. Zhang, L. Song, M. Xu, H. Cheng, Y. Zhao, Z. Zhang, F. Liu and L. Qu, Enabling Fast-charging Selenium-based Aqueous Batteries via Conversion Reaction with Copper Ions, *Nat. Commun.*, 2022, **13**, 1863.
- 53 S. K. Sandstrom, H. Jiang, M. Lucero, Y. Xu, T. C. Gallagher, M. Cao, Z. Feng and X. Ji, Reversible Electrochemical Conversion from Selenium to Cuprous Selenide, *Chem. Commun.*, 2021, **57**, 10703–10706.
- 54 J. Long, J. Dong, X. Wang, Z. Ding, Z. Zhang, L. Wu, Z. Li and X. Fu, Photochemical Synthesis of Submicron- and Nano-Scale Cu<sub>2</sub>O Particles, *J. Colloid Interface Sci.*, 2009, **333**, 791–799.
- 55 J. Y. Morimoto and B. A. Degraff, Photochemistry of the Copper(II)-Malonate System. A “Sensitized” Reaction, *J. Phys. Chem.*, 1972, **76**, 1387–1388.
- 56 J. Y. Morimoto and B. A. Degraff, Photochemistry of Copper Complexes. Copper(II) Malonate System, *J. Phys. Chem.*, 1975, **79**, 326–331.
- 57 P. Natarajan and G. Ferraudi, Photochemical Properties of Copper(II)-Amino Acid Complexes, *Inorg. Chem.*, 1981, **20**, 3708–3712.
- 58 S. Liu, Z. Zhang, J. Bao, Y. Lan, W. Tu, M. Han and Z. Dai, Controllable Synthesis of Tetragonal and Cubic Phase Cu<sub>2</sub>Se Nanowires Assembled by Small Nanocubes and Their Electrocatalytic Performance for Oxygen Reduction Reaction, *J. Phys. Chem. C*, 2013, **117**, 15164–15173.

